Internal-friction peaks of hydrogen in amorphous and crystalline $Co_{33}Zr_{67}$

1991 J. Phys.: Condens. Matter 3 2005

(http://iopscience.iop.org/0953-8984/3/13/004)

J. Phys.: Condens. Matter 3 (1991) 2005–2020. Printed in the UK

Internal-friction peaks of hydrogen in amorphous and crystalline $Co_{33}Zr_{67}$

H-R Sinning
Institut für Werkstoffe, Technische Universität Braunschweig, Langer Kamp 8, D-3300 Braunschweig, Federal Republic of Germany

Received 21 September 1990

Abstract. The hydrogen-induced internal-friction spectra, for hydrogen concentrations below 10 at.%, are measured in the different crystallization stages of amorphous $Co_{33}Zr_{67}$ at various temperatures and frequencies using the vibrating-reed technique. Four internal-friction peaks are observed and analysed with respect to the underlying relaxation mechanisms. Three of them can be attributed to Snoek-type relaxation processes caused by thermally activated jumps of H atoms between neighbouring Zr_4 tetrahedral sites in (i) the amorphous phase, (ii) the grain boundaries of a metastable, nanocrystalline state of cubic $CoZr_2$, and (iii) the crystal lattice of the tetragonal $CoZr_2$ equilibrium phase, respectively. Structural and microstructural implications of these results are outlined.

1. Introduction

The appearance of a characteristic internal-friction (IF) peak associated with the presence of absorbed hydrogen is a common feature of many metallic glasses; examples can be found in the literature for both metal–metal [1–3] and metal–metalloid glasses [3–5]. The origin of this peak is usually ascribed to a Snoek-type (i.e. single-atom reorientation) relaxation mechanism where the H atom is jumping between orientationally distinguishable 'interstitial' sites. This is in contrast to crystalline materials, especially BCC metals (the crystal structure underlying the 'original' Snoek relaxation of C in α-Fe), where a hydrogen Snoek relaxation is hard to observe; Berry and Pritchet [5] even claimed that the IF peak in metallic glasses was the first known example of a hydrogen Snoek relaxation. These authors also point out that, for reasons of sample preparation, the crystallization of amorphous samples may be a useful general approach to study hydrogen in intermetallic compounds.

The binary group VIII–group IV transition-metal glasses (Ni–Ti, Ni–Zr, Co–Zr, etc) may be considered as good candidate glasses for such studies for two reasons: (i) these materials are usually able to absorb very large quantities of hydrogen and (ii) a lot of binary intermetallic phases can be produced by crystallization from the glassy state. For basic investigations, the most interesting case here is a polymorphic type of crystallization without any change in composition; the alloy $Co_{33}Zr_{67}$ crystallizing into the intermetallic compound $CoZr_2$ is thought to be one such model system [6].

However, it has been found in several crystallization studies [7–10] that $CoZr_2$ does not crystallize immediately into the tetragonal equilibrium structure (C16, $CuAl_2$ type

0953-8984/91/132005 + 16 $03.50

[11]) but first into a metastable phase of complex cubic structure ($E9_3$, $NiTi_2$ type with 96 atoms/cell [9]). The grain size produced by this first crystallization reaction between 350 and 450 °C decreases strongly with increasing reaction temperature, so that annealing above 400 °C (or heating rates above 2 K min^{-1}) results in a 'nanocrystalline' structure with grain diameters of only a few nanometres [10]. The transition into the tetragonal equilibrium phase then occurs in two further exothermic reactions at higher temperatures up to 650 °C (with considerable scatter in reaction temperatures between different ribbons). Between these two reactions, a very complicated, highly defective microstructure consisting of at least both the cubic and tetragonal $CoZr_2$ phases ('mixed state') is observed. The real mechanism of this cubic/tetragonal transition is still unknown.

Thus, in $Co_{33}Zr_{67}$ the hydrogen-induced internal friction can be studied in at least one amorphous and two intermetallic crystalline phases of the same composition, including the nanocrystalline state that presently enjoys a growing interest in materials science [12]. In a preliminary paper, an IF peak appearing in both the amorphous and the nanocrystalline state was discovered but not yet clearly identified as a hydrogen effect [13].

In the present work, the hydrogen-induced internal-friction spectra in $Co_{33}Zr_{67}$ are investigated in the amorphous state and in the different crystallization stages. Only hydrogen concentrations between 10^{-3} and 10^{-1} H/Me (0.1–10 at.%) are considered. An attempt is made to identify the different microscopic relaxation mechanisms underlying the observed IF peaks. Possible applications to resolve structural and microstructural questions are finally outlined.

2. Experimental details

The amorphous $Co_{33}Zr_{67}$ alloy was produced in the form of 1–2 mm wide and about 35 μm thick ribbons by melt spinning under vacuum†. The as-quenched material already contained between 0.1 and 0.3 at.% hydrogen as an impurity, as was analysed by heat extraction. Part of the amorphous samples were additionally charged with hydrogen either electrolytically (in H_3PO_4 + glycerine) or from the gas phase. In the latter case, the samples usually remained in their vibrating-reed holder so that internal-friction measurements before and after charging were possible on the same sample without any change in geometry.

The internal friction Q^{-1} and resonance frequency f were measured on flexural vibrations (10^2–10^4 Hz) using the vibrating-reed technique. A schematic block diagram of the apparatus working with electrostatic excitation and an HF detection circuit is shown in figure 1. The samples were mounted horizontally in the 'cantilever beam' configuration, i.e. as a vibrating reed tightly clamped in a holder at one end. The holder with the mounted sample could be removed from the apparatus and then, for instance, inserted into the hydrogen-gas charging device.

The sample temperature was varied by means of a cylindrical radiation furnace and measured with a thermocouple situated in a small hole in the sample holder, close to the sample. For temperatures below room temperature, the whole vacuum container with sample and furnace was immersed in liquid nitrogen.

† The production of the amorphous material was carried out by D Plischke at the 'Kristallabor der physikalischen Institute', University of Göttingen.

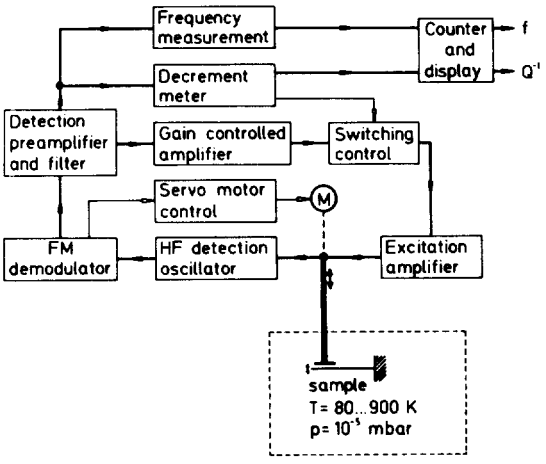

Figure 1. Simplified block diagram of the vibrating-reed apparatus.

A problem in such a configuration is the presence of temperature gradients along the sample, which are very hard to avoid. They cause a systematic error in the measurement of internal-friction peak temperatures, especially in those cases where harmonics are used to obtain higher frequencies. An incorrect determination of activation energies may then result from such gradients. For this reason, a temperature correction was applied to those internal-friction data that were obtained by using harmonics. Details of this correction and its influence on activation energy values are given in the appendix.

All heat treatments applied to the samples were performed *in situ* in the vibrating-reed apparatus. In most cases, the changes of internal friction and resonance frequency (or Young's modulus) during a heat treatment were recorded in order to monitor the transformations within the sample. These were also checked by differential scanning calorimetry (DSC) and transmission electron microscopy (TEM).

3. Results

3.1. Development of the internal-friction spectrum during crystallization

Figure 2 shows a typical example of the change in the temperature spectrum of internal friction below 400 K during the crystallization sequence of $Co_{33}Zr_{67}$. According to the accompanying characterization of the material by DSC, TEM and Young's modulus, the four IF spectra in figure 2 belong to: (*a*) the amorphous state, (*b*) the nanocrystalline state of $CoZr_2$ (cubic), (*c*) the complicated 'mixed state' mentioned above, and (*d*) an almost complete transformation into $CoZr_2$ (tetragonal) at the temperature limit of the vibrating-reed apparatus (640 °C). The four IF peaks observed successively in these crystallization stages have been numbered in the sequence of their appearance during crystallization of as-quenched specimens. Each of these peaks was investigated thoroughly by varying the hydrogen content, frequency and microstructural parameters.

A global overview of the effect of a strong hydrogen charging on the sequence of IF spectra may be obtained by comparing figures 2 and 3. In figure 3, the procedure was as

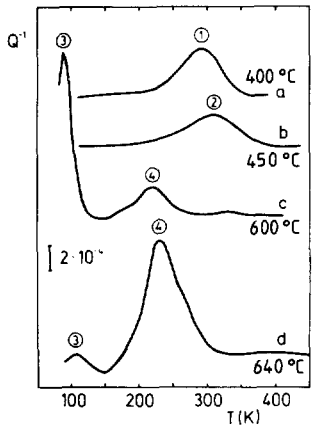

Figure 2. Internal-friction peaks in $Co_{33}Zr_{67}$ at a frequency of 580 ± 80 Hz after heating at a constant heating rate of 1 K min^{-1} ((*a*) and (*b*)) or 2 K min^{-1} ((*c*) and (*d*)) up to (*a*) 400 °C, (*b*) 450 °C, (*c*) 600 °C and (*d*) 640 °C.

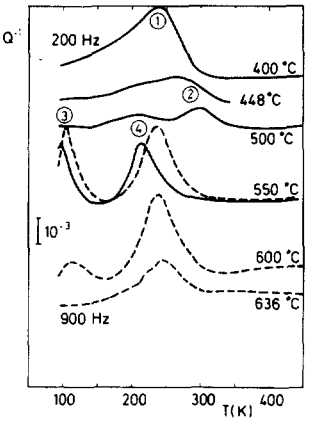

Figure 3. Internal-friction peaks of a $Co_{33}Zr_{67}$ specimen charged electrolytically with hydrogen and then heated at 1 K min^{-1} up to the temperatures indicated. After heating to 550 °C, the specimen was shortened so that the fundamental frequency of vibration changed from 200 to 900 Hz.

follows: an as-quenched specimen was charged electrolytically with a high, but undefined, hydrogen content and partially degassed by thermal treatments within the amorphous state. (This is only possible for high hydrogen contents; in contrast, the low, initial hydrogen content of the as-quenched material does not degas until heating to well beyond the melting point.) The specimen was then annealed successively to the temperatures indicated in the figure; after each annealing treatment, the low-temperature IF spectrum was measured several times at different frequencies (fundamental mode and harmonics, not shown in figure 3). After heating to 550 °C, the specimen was cut to a shorter length to obtain a higher fundamental frequency, leading to the temperature shift between the full and broken curves in figure 3.

The influence of hydrogen on each IF peak will be considered in detail in the next section. In addition, the sequence of the peaks is different in figures 2 and 3: after hydrogen charging, peak 4 is observed earlier than peak 3, and both peaks 3 and 4 appear at lower annealing temperatures than without hydrogen charging. This is clearly due to the influence of hydrogen on crystallization occurring at higher hydrogen concentrations, which should be kept in mind for the following sections. The effect is also observed in the characteristic modulus changes during annealing. The TEM micrographs in figure 4 show that hydrogen mainly favours the tetragonal $CoZr_2$ equilibrium phase: after charging with hydrogen, this phase obviously forms already from the amorphous state in competition with the metastable cubic phase (figure 4(*b*)), whereas without additional hydrogen charging only cubic crystals are observed for a similar heat treatment (figure 4(*a*)).

3.2. Phenomenological characterization of the observed internal-friction peaks

We have pointed out earlier that the IF peak in the amorphous state (peak 1), as measured without additional hydrogen charging, is almost unaffected by structural relaxation

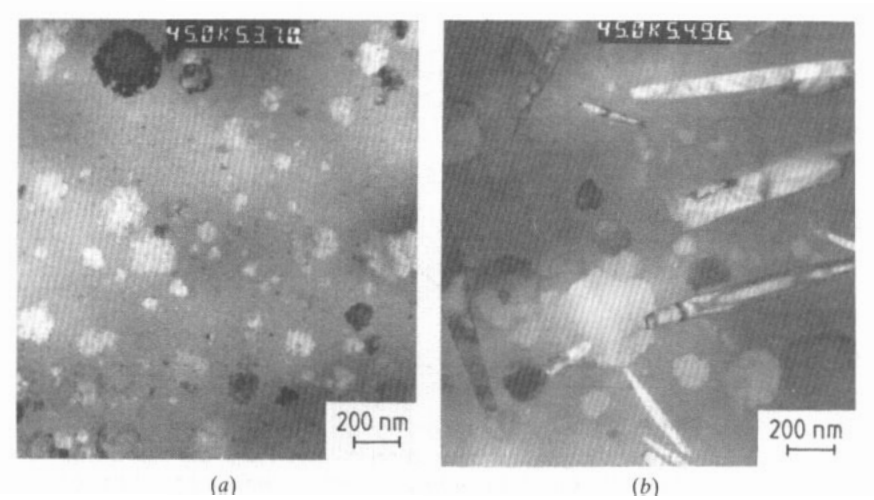

Figure 4. Transmission electron micrographs of $Co_{33}Zr_{67}$ annealed isothermally at 380 °C into a partially crystallized state. (*a*) Without hydrogen charging; crystals of cubic $CoZr_2$ in the amorphous matrix. (*b*) After hydrogen charging from the gas phase (120 bar, 100 °C); globular crystals of cubic $CoZr_2$ and rods or plates of tetragonal $CoZr_2$ in the amorphous matrix.

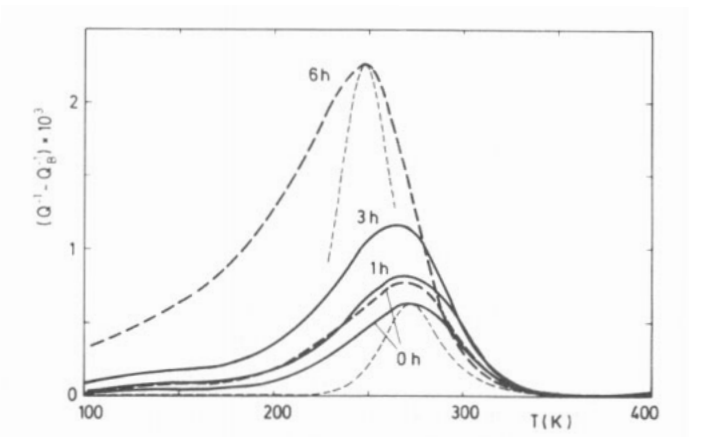

Figure 5. Effect of hydrogen charging on peak 1 in amorphous $Co_{33}Zr_{67}$ at a frequency $f = 300$ Hz. Two samples (full and thick broken curves, respectively) were first measured without hydrogen charging (0 h), then exposed to hydrogen gas of 120 bar at 100 °C for the times indicated, and measured again. The thin broken curves are Debye peaks expected for a single relaxation time [14], which were calculated using the activation energy values of figure 11.

treatments, i.e. heat treatments within the amorphous state [13]. However, later measurements have shown that this is not always the case but that as-quenched samples occasionally show a higher peak, which can then be reduced to the 'normal' height of about 5×10^{-4} by annealing. For the sake of reproducibility, we will consider in the following only IF measurements on amorphous samples that were obtained in a structurally relaxed condition.

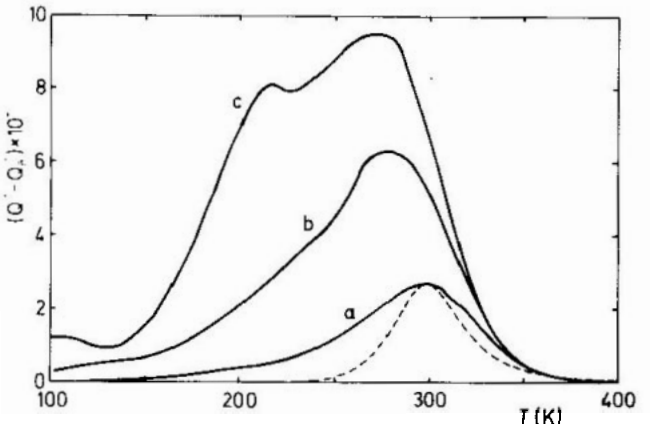

Figure 6. Effect of hydrogen on peak 2 observed in the 'nanocrystalline' state of $CoZr_2$ ($f = 300$ Hz): (*a*) without hydrogen charging, specimen crystallized by heating at 2 K min^{-1} to 460 °C; (*b*) specimen exposed to H_2 gas of 120 bar at 100 °C for 3 h and then crystallized by heating at 2 K min^{-1} to 455 °C; (*c*) specimen severely charged electrolytically, then partially degassed and crystallized by isothermal annealing for 6 h at 404 °C. The thin broken curve is the Debye peak as in figure 5.

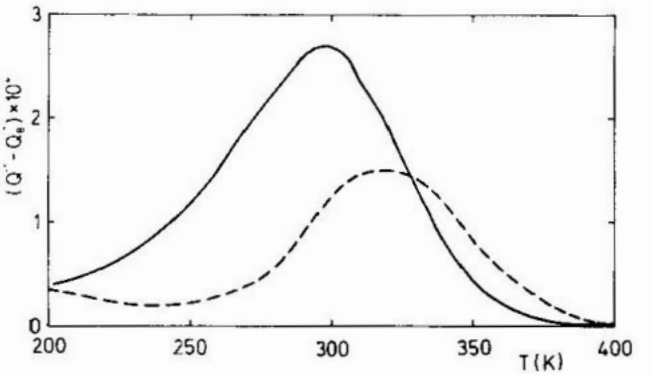

Figure 7. Influence of the grain size in cubic $CoZr_2$ on peak 2 ($f = 300$ Hz; no additional hydrogen charging). Full curve: after crystallization by heating at 2 K min^{-1} to 460 °C (curve (*a*) in figure 6); truly nanocrystalline state with an average grain size of less than 10 nm. Broken curve: after isothermal crystallization for 120 h at 350 °C; grain size about 200 nm [10].

The influence of successive hydrogen charging treatments from the gas phase on peak 1 is shown in figure 5. For comparison of the different measurements, in this and the following plots a linear background Q_B^{-1} has been subtracted from the raw internal-friction data. The peak height is found to grow continuously with increasing charging time, combined with a shift to lower temperatures. This behaviour and the observed width and asymmetry of the measured peaks, compared to a Debye peak with a single relaxation time [14], is well known for hydrogen in metallic glasses [1–5].

A very similar behaviour is also observed for peak 2, the IF peak measured after the first crystallization reaction (figure 6). However, as hydrogen charging was done in the

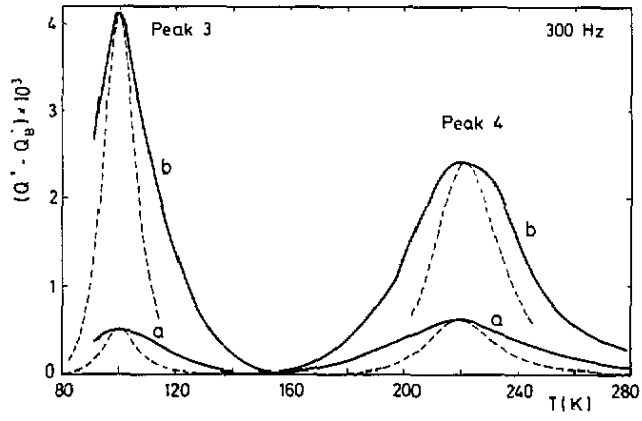

Figure 8. Effect of hydrogen on peaks 3 and 4 (f = 300 Hz): (*a*) without hydrogen charging, specimen heated at 2 K min^{-1} up to 640 °C; (*b*) specimen exposed to H_2 gas of 120 bar at 100 °C for 6 h and then heated at 2 K min^{-1} up to 550 °C. The thin broken curves are Debye peaks as in figure 5.

amorphous state, the above-mentioned influence of hydrogen on the crystallization itself is superimposed on the increase of peak 2, resulting in a premature appearance of peak 4 as a shoulder on peak 2 at the highest hydrogen content in figure 6.

A further parameter that may have an influence on peak 2 is the grain size after the first crystallization reaction. In our material, the average grain diameter could be varied from a few nanometres (truly nanocrystalline state) to values of about 200 nm by different annealing conditions [10]. As figure 7 shows, the peak height increases with decreasing grain size, but only by about a factor of 2 over the whole range of grain sizes investigated. Again, the larger peak is situated at somewhat lower temperatures than the smaller one.

The effect of hydrogen charging on peaks 3 and 4, i.e. the IF peaks belonging to the later crystallization stages, is shown in figure 8. These specimens were annealed into the 'mixed state' during the cubic/tetragonal transformation to show both peaks simultaneously. It is again the influence of hydrogen on crystallization that is responsible for the difference between the annealing treatments chosen in figure 8. The height of both peaks again increases markedly with hydrogen content; however, contrary to peaks 1 and 2, these peaks are now more symmetrical (although still broader than a Debye peak) and do not shift in temperature.

Thus, all four IF peaks described in this work are strongly enhanced by increasing the hydrogen content. Because of experimental problems and scatter between individual samples, we are not yet able to correlate the measured peak heights quantitatively to exact hydrogen concentration values from heat extraction analysis; the largest content in figures 5 to 8 may be estimated to be a few atomic per cent.

3.3. Thermal activation analysis

Whereas in the last section all internal-friction peaks have been considered at a constant frequency of 300 Hz, we will now evaluate the frequency dependence. When the frequency is raised, all four peaks observed here shift to higher temperatures, which

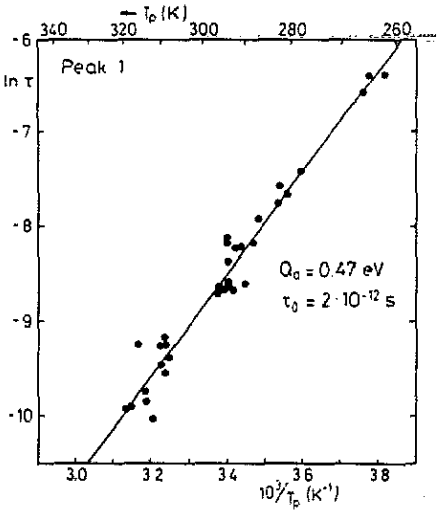

Figure 9. Arrhenius plot of the frequency shift of peak 1, showing all the data obtained on structurally relaxed, amorphous samples without hydrogen charging.

indicates a thermally activated process. An example for peaks 3 and 4 has been shown in figure 3 (the '550 °C' spectrum); for peaks 1 and 2, this has already been demonstrated earlier [13]. This frequency shift of the peak temperature was investigated systematically for frequencies between 10^2 and 10^4 Hz, by varying the length of the samples as well as by using harmonics. As already mentioned, in the latter case a temperature correction was applied to account for thermal gradients (see appendix).

The average activation energy Q_a and pre-exponential factor τ_0 were evaluated in the usual way [14] from Arrhenius plots of ln τ versus $1/T_p$, where $\tau = 1/2\pi f$ and T_p is the peak temperature. For the amorphous state in a structurally relaxed condition (peak 1), a common relationship was observed even for different samples, so that a single straight line could be fitted to all the data (figure 9). In contrast, peak 2 shows a significant additional scatter in T_p between individual samples (figure 10), which would cause an error in activation parameters if evaluated like peak 1 (broken line in figure 10). In that case it is necessary to determine the parameters Q_a and τ_0 for each sample separately (using only samples where at least two measurements at different frequencies have been made) and then to take the average of these individual parameters, which is represented by the thick, full line in figure 10. A similar procedure was applied to the evaluation of peaks 3 and 4.

In figure 11, the activation parameters Q_a and τ_0 of peaks 1 and 2 have been plotted as a function of the peak height ΔQ_p^{-1}, which may be regarded as a qualitative measure of the hydrogen content, with maximum values estimated near 10 at.%. (In this concentration range, the relationship between hydrogen content and ΔQ_p^{-1} is still monotonic.) It is not yet clear whether the exact shapes of the curves in figure 10 (especially the minimum in τ_0) are statistically significant; however, the decrease of Q_a with increasing hydrogen content is beyond doubt. Such behaviour is also known from the literature [1, 5].

The main feature to be learned from figure 11 is that there is apparently no difference in activation parameters between peaks 1 and 2, the IF peaks measured in the amorphous and the 'nanocrystalline' states: both sets of points fall on the same curves. This will be discussed further below.

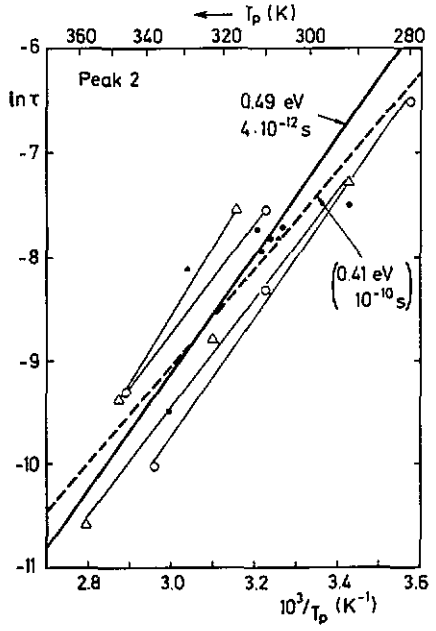

Figure 10. Arrhenius plot of the frequency shift of peak 2. Open symbols and thin lines: samples measured at least at two different frequencies. Small, full symbols: samples measured at only one frequency. The thick broken line was fitted to all data points, whereas the thick full line represents the average of the Q_a and τ_0 values determined individually from the thin lines.

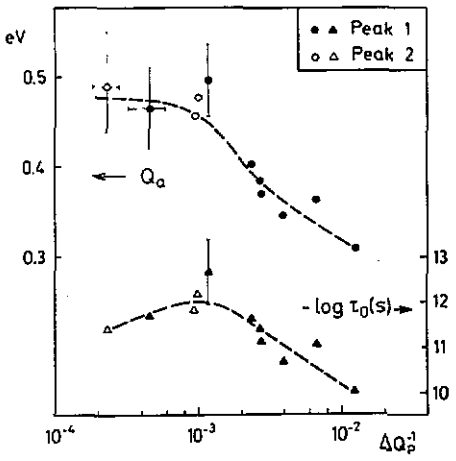

Figure 11. Activation energy Q_a and pre-exponential factor τ_0 for peaks 1 and 2, plotted as a function of the peak height ΔQ_p^{-1}.

For peaks 3 and 4, a dependence of the activation parameters on the peak height or hydrogen content could not be observed. The average values were determined as

$Q_a = 0.17 \pm 0.02$ eV $\quad \log \tau_0 = -11.8 \pm 0.6 \quad (\tau_0 = 2 \times 10^{-12}$ s)

for peak 3 and

$Q_a = 0.41 \pm 0.06$ eV $\quad \log \tau_0 = -12.6 \pm 1.2 \quad (\tau_0 = 3 \times 10^{-13}$ s)

for peak 4. It should be mentioned that the values for peak 4, although belonging to the

last stage of crystallization, are of the same order as those of peak 1 in the amorphous state (figure 11).

4. Discussion

4.1. Anelastic relaxation mechanisms

The experimental results presented above justify the assumption that all four internal-friction peaks observed in this work on amorphous and crystalline $Co_{33}Zr_{67}$ are caused by hydrogen-induced, thermally activated relaxation processes. We will now consider the microscopic nature and atomic mechanism of each of these relaxation processes.

4.1.1. Peak 1 (amorphous state). As already mentioned earlier, the occurrence of a hydrogen-induced IF peak based on a Snoek-type relaxation mechanism is a rather general phenomenon common to many metallic glasses of quite different chemical compositions. All the properties of our 'peak 1' described above, including the values of the activation parameters, agree well with the results known from the literature [1–5] and thus confirm that we have the same phenomenon here.

Neutron diffraction studies of hydrogen in amorphous Ni–Zr [15] and Cu–Ti [16] have shown that the H atoms, in the concentration range of interest here, occupy only tetrahedral sites surrounded by four Zr or Ti atoms, respectively. Based on these observations, Stolz *et al* [2] interpreted their IF results of hydrogen in $Ni_{35}Ti_{65}$ using the concept of tetrahedral sites and found that up to concentrations of 0.25 H per metal atom (H/Me) the Ti_4 tetrahedra are filled with hydrogen. It was argued that in these and similar materials chemical affinity may be regarded as the primary factor governing the occupation of sites by H atoms, whereas the topological (structural) distribution and distortion of sites are only important in a secondary manner [17]. The same behaviour can be expected for $Co_{33}Zr_{67}$, which is chemically similar to $Ni_{35}Ti_{65}$.

Thus, we attribute our peak 1 in amorphous $Co_{33}Zr_{67}$ to a Snoek-like relaxation caused by thermally activated jumps of H atoms between neighbouring Zr_4 tetrahedra. To give rise to such a Snoek relaxation, these tetrahedra must be distorted by the amorphous structure in such a way that the neighbouring sites are orientationally distinguishable.

4.1.2. Peak 2 (cubic $CoZr_2$/nanocrystalline state). The argument of chemical affinity given above is certainly not restricted to amorphous alloys but may be important for the occupation of interstitial sites by hydrogen in crystalline intermetallic compounds as well. If we consider the possibility of a Snoek relaxation in crystalline $CoZr_2$, we should therefore first look for interstitial sites surrounded only by Zr atoms.

In the metastable, complex-cubic $CoZr_2$ phase with $E9_3$ ($NiTi_2$) structure crystallizing first, the only interstitial sites with a pure Zr coordination shell are isolated, regular Zr_6 octahedra [18]. Both the high symmetry of these sites and the lack of directly neighbouring, equivalent sites make a Snoek relaxation of H atoms dissolved in these sites impossible. Thus, at low H concentrations we do not expect a Snoek relaxation from hydrogen dissolved in the $E9_3$ crystal lattice. If at all, such a contribution could only be expected at concentrations high enough to occupy interstitial sites with a mixed Zr/Co coordination.

We therefore have convincing evidence to postulate that the IF peak 2 is caused by hydrogen atoms dissolved in the grain boundaries of cubic $CoZr_2$, especially in the nanocrystalline state where the volume fraction of grain boundaries can reach 50% [10]. The identity of the activation parameters of peaks 1 and 2 observed in figure 11 then strongly suggests that the relaxation mechanism is the same as in amorphous $Co_{33}Zr_{67}$. This would imply that the symmetry and distortion of the Zr_4 tetrahedra are almost the same in both cases or, more generally speaking, that the structure of the grain boundaries in nanocrystalline $CoZr_2$ is similar to that of the glass.

The assumption of a relaxation mechanism located in the grain boundaries is also supported by the grain size dependence of the peak height (figure 7): the decrease in peak height with increasing grain size could not be understood if the peak were ascribed to hydrogen dissolved in the undisturbed crystal lattice.

On the other hand, this decrease in peak height is much weaker than expected from the volume fraction of grain boundaries, indicating a partially compensating effect like a segregation of hydrogen at the grain boundaries. Such a segregation is indeed often assumed and has been observed experimentally in the case of palladium [19].

4.1.3. Peak 3 ('mixed state'). The interpretation of peak 3 must remain rather speculative. As it only occurs in the intermediate, complicated 'mixed state' during the crystallization sequence of $Co_{33}Zr_{67}$, it can be attributed neither to the cubic nor to the tetragonal phase of $CoZr_2$. If no other, still unidentified, phases are present in this 'mixed state', the interaction of hydrogen with defect structures produced during the cubic/tetragonal transformation would be the most plausible explanation for peak 3. As the activation parameters of this peak are well defined and do not change with hydrogen content, such defect structures must be very regular and offer well defined sites for the H atoms. This could be imagined, for instance, for the case of special, crystallographically oriented cubic/tetragonal interfaces with a regular structure.

4.1.4. Peak 4 (tetragonal $CoZr_2$). The comparison of the measured IF spectra with parallel crystallization studies have clearly shown that the occurrence of peak 4 is directly connected with the presence of the tetragonal $CoZr_2$ equilibrium phase. A detailed description of the C16 ($CuAl_2$-type) crystal structure of this phase can be found in the work of Havinga *et al* [11]. To check the possibility of a hydrogen Snoek relaxation, it is necessary to take a closer look at this structure.

Figure 12 shows the (100) and (001) projections of the C16 structure taken from [11]. For reasons of chemical affinity mentioned above, the positions of the Zr atoms are particularly interesting. There are four slightly different Zr–Zr nearest-neighbour distances with

$$d_1 = 3.07\ \text{Å} \qquad d_3 = 3.51\ \text{Å} \qquad a = 6.364\ \text{Å}$$

$$d_2 = 3.11\ \text{Å} \qquad d_4 = 3.34\ \text{Å} \qquad c = 5.518\ \text{Å}$$

for $CoZr_2$ [11]. If the shortest distances d_1 and d_2 are considered preferentially, it is seen that the Zr atoms form two sets of mutually orthogonal planes with a dense packing of hexagons (honeycomb structure), parallel to (110) and $(1\bar{1}0)$, respectively. The Co atoms are situated in the channels parallel to the c axis, which are formed by this interlocking honeycomb structure.

In addition to the positions of the Co and Zr atoms, the interstitial sites with purely Zr neighbours have also been marked in figure 12. These are all tetrahedral sites, but

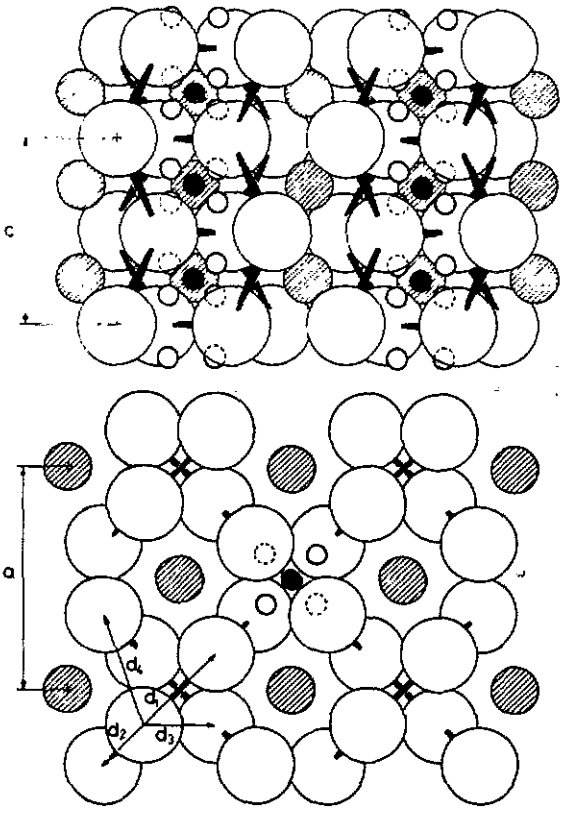

Figure 12. The (100) (*a*) and (001) (*b*) projections of the C16-type structure of tetragonal $CoZr_2$ [11]. The big, white atoms represent Zr, the smaller, shaded atoms Co. The Zr atoms belonging to the same hexagon network have been graphically interlinked with each other. Indicated also are the positions of the Zr_4 tetrahedral interstitial sites: ●, type 1 site; ○, type 2 site (see text).

two types of Zr_4 tetrahedra distorted in different ways can be distinguished: one with two edges of length d_1 and four edges of length d_3 (type 1), and the other with one d_1, one d_2, two d_3 and two d_4 edges (type 2). The type 1 tetrahedral sites form a sublattice equivalent to that of the Co atoms but displaced from the latter by a vector of $(a/2)(100)$; these sites have the same symmetry as the tetragonal crystal structure and thus cannot contribute to a Snoek relaxation by themselves. However, each type 1 site is surrounded by four type 2 sites having a lower symmetry than the crystal and different orientations, which is necessary for a Snoek relaxation. These groups of five Zr_4 tetrahedral sites are arranged in isolated chains along the *c* direction like the Co atoms, with each type 2 site neighbouring one type 1 and one type 2 site (and two $CoZr_3$ tetrahedra). It is interesting to note that in this structure long-range hydrogen diffusion is only possible in the *c* direction as long as the H atoms are only occupying the Zr_4 tetrahedra.

A Snoek relaxation can be expected for jumps of hydrogen atoms between type 1 and type 2 sites as well as for jumps between neighbouring type 2 sites. We regard these jumping processes as responsible for our internal-friction peak 4 in tetragonal $CoZr_2$.

It cannot be said at the moment which of these jumps ($1 \leftrightarrow 2$ or $2 \leftrightarrow 2$) is the dominant one; in a polycrystal, this may well be different in grains of different orientation, giving rise to a distribution of relaxation times in such a specimen. This could account for the observed broadening of peak 4 compared to a Debye peak with a single relaxation time.

The above-mentioned, somewhat curious similarity of the activation parameters of peaks 1 and 4 now finds its natural explanation: both relaxation processes have indeed been attributed to qualitatively the same mechanism: the jump of hydrogen atoms between neighbouring Zr_4 tetrahedra.

4.2. Conclusions and applications

Among the four internal-friction peaks of hydrogen in $Co_{33}Zr_{67}$ described in this work, we have concluded that three can be ascribed to basically the same microscopic event, the thermally activated jump between neighbouring Zr_4 tetrahedra: peak 1 in the amorphous phase; peak 2 in the grain boundaries of the metastable, cubic $CoZr_2$ phase; and peak 4 in interstitial sites within the tetragonal crystal lattice of the $CoZr_2$ equilibrium phase. As these three phases of the same composition transform into each other during a crystallization sequence, the different IF spectra may be studied on a single specimen, without removing it from its holder, so that the different relaxation processes can be compared to each other under very reproducible conditions. This outstanding situation gives rise to applications of the internal-friction spectra with respect to both structural and microstructural questions.

4.2.1. Structural applications. The structural applications of hydrogen-induced IF peaks make use of the elementary jumping processes of hydrogen atoms as a probe to monitor structural features of the hydrogen-absorbing phase. For instance, a dependence of activation energies (figure 11) and peak heights on the hydrogen content in the amorphous phase may be compared with distributions of site energies predicted from structural models [2, 17]. What is exceptional for $Co_{33}Zr_{67}$ and what we want to emphasize here is, however, the possibility of studying structural units like the Zr_4 tetrahedra in a comparative manner when they are embedded in different phases with quite different long- or short-range order. For instance, geometrical knowledge about the interstitial sites in the C16 crystal lattice might also provide information on the amorphous structure and on the modification of this structure in the grain boundaries of the nanocrystalline state.

A first, qualitative application in this sense has been the conclusion drawn above from figure 11, that the nanocrystalline grain boundary structure is similar to the amorphous one, in contrast to what has been claimed for pure, nanocrystalline iron [20]. A further, structural conclusion can be drawn from the peak positions in figure 7, provided our interpretation of peak 2 is correct: the grain boundary segregation of hydrogen, needed to explain the peak heights for the different grain sizes, would result in a lower peak temperature for the larger grain size due to the local increase in hydrogen concentration if the grain boundary structure were independent of grain size. The fact that this is not observed in figure 7, but that there is even a slight effect in the opposite direction, may be taken as an indication of a grain size dependence of the structure of the grain boundaries.

A refinement of the structural information available from hydrogen-induced IF data might be expected from a more systematic and quantitative variation of the hydrogen content, which would also include hydrogen charging in the different crystalline states,

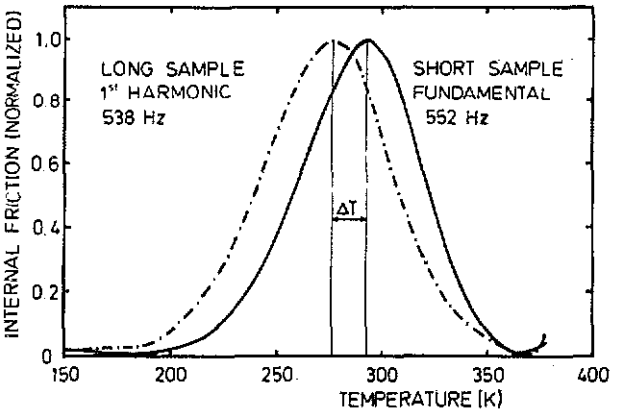

Figure 13. Shift of the internal-friction peak in amorphous $Co_{33}Zr_{67}$ (peak 1) due to thermal gradients: a long sample with a fundamental frequency below 100 Hz was measured on heating at 1 K min^{-1} using the first harmonic and then cut to a shorter length so that a second measurement at the same frequency (545 ± 7 Hz) could be made in the fundamental mode.

in order to separate the structural information from a possible influence of hydrogen on the phase transformations.

4.2.2. Microstructural applications. Each of the IF peaks 1, 2 and 4 has been clearly identified with one of the phases appearing in the crystallization sequence of amorphous $Co_{33}Zr_{67}$. Peak 3, although less well described, can clearly be attributed to a certain transitional, multiphase and defect-rich stage during that sequence. These properties make the hydrogen IF spectrum phenomenologically suitable to monitor the phase transformations in this alloy and to detect and identify a certain phase even in a complicated microstructure. There are advantages of this method with respect to x-ray or electron diffraction, at least under the special conditions of the Co–Zr alloy [21]. Examples have been given above in figures 3 and 6, showing the response of the IF spectrum to the influence of an enhanced hydrogen content on crystallization. Another, more pronounced example of this effect can be found in [21].

Acknowledgments

Thanks are due to Professor H C Freyhardt and to D Plischke for production and supply of the amorphous $Co_{33}Zr_{67}$ alloy, and to M M Nicolaus for her help in transmission electron microscopy and valuable discussions.

Appendix. The effect of temperature gradients

In the set-up of the vibrating-reed experiments (vacuum, continuous heating by radiation, thin samples clamped in a comparatively thick holder), we cannot expect a uniform temperature of the whole sample but must admit temperature gradients, e.g. when the sample holder is heated up more slowly than the free end of the sample due to

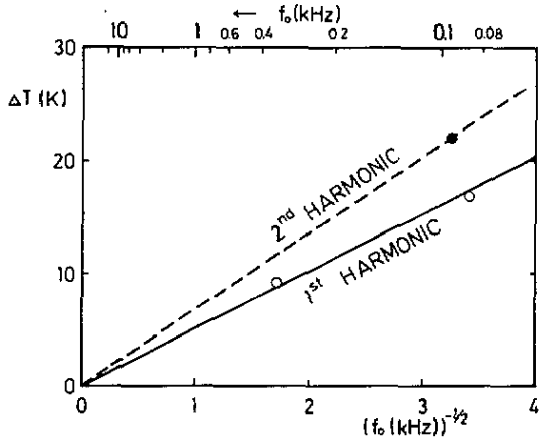

Figure 14. Correction of the peak temperatures of peak 1 for measurements using the first and second harmonic vibrations (f_0 = fundamental frequency).

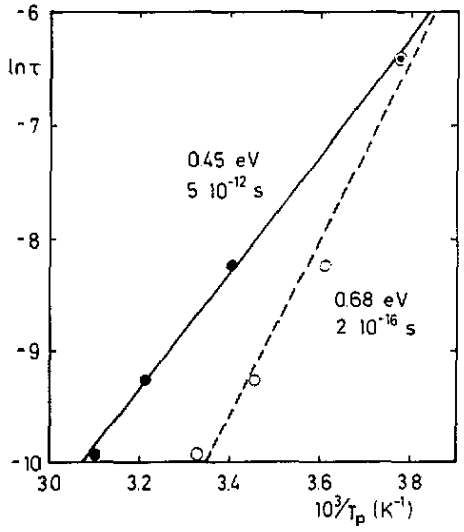

Figure 15. Arrhenius plot of the frequency shift of peak 1 (cf section 3.3), measured on a single specimen in different vibration modes. Open symbols, uncorrected data; full symbols, corrected data.

the difference in thermal capacity. For the kinetic analysis based on the frequency shift of the IF peak temperatures T_p [14], it is important to know at least the relative influence of such thermal gradients on the measurement of T_p when the frequency is varied by changing either the length of the sample or the mode of vibration.

In flexural vibrations, the most important contributions to the measured damping come from those parts of the sample that are close to a maximum in strain amplitude. In the fundamental mode, there is only one such maximum at the clamped end of the sample, i.e. close to the point where the temperature is measured. In that case, the relevant error in temperature measurement can be expected to be rather small. In the higher harmonics, however, there are several strain maxima along the sample, so that in the case of a temperature gradient the measured (average) internal friction corresponds to another temperature than in the fundamental mode. Figure 13 shows that this can indeed lead to a considerable shift ΔT of the measured IF peak. This 'gradient shift' is superimposed on the 'frequency shift' when the frequency is varied

by choosing different vibration modes (which is advantageous, as a non-destructive method, compared to cutting the sample to a shorter length) and must be subtracted from the measured data in order to obtain correct activation parameters.

It is plausible to assume that the correction ΔT is proportional to the length of the sample when all other relevant parameters are held constant. This gives straight lines in a plot of ΔT versus $f_0^{-1/2}$, which can then be used for correcting measurements obtained on harmonics belonging to arbitrary fundamental frequencies f_0 (figure 14). In view of the variety of parameters influencing the thermal gradients, it is important to determine this gradient correction for each IF peak separately, and to maintain reproducible conditions with respect to specimen composition, geometry, preannealing and heating rate.

The Arrhenius plot in figure 15 shows that the corrected data points fall much better on a straight line than the uncorrected ones, and demonstrates the substantial influence of the correction on the evaluated activation parameters. Although it is possible that this gradient effect might be especially large in the present case, the apparent lack of reference to corresponding corrections in the literature gives rise to some caution with respect to published activation parameters from similar internal-friction studies.

References

[1] Agyeman K, Armbruster E, Künzi H U, Das Gupta A and Güntherodt H-J 1981 *J. Physique Coll.* **42** (C5) 535
[2] Stolz U, Weller M and Kirchheim R 1986 *Scr. Metall.* **20** 1361
[3] Berry B S and Pritchet W C 1981 *Scr. Metall.* **15** 637
[4] Yoshinari O, Koiwa M, Inoue A and Masumoto T 1983 *Acta Metall.* **31** 2063
[5] Berry B S and Pritchet W C 1984 *Nontraditional Methods in Diffusion* ed G E Murch, H K Birnbaum and J R Cost (Warrendale, PA: Metallurgical Society of AIME) pp 83–110
[6] Blank-Bewersdorff M and Köster U 1988 *Mater. Sci. Eng.* **97** 313
[7] Buschow K H J 1982 *J. Less-Common Met.* **85** 221; 1984 *J. Phys. F: Met. Phys.* **14** 593
[8] Jansson K, Nygren M and Östlund A 1984 *Mater. Res. Bull.* **19** 1091
[9] Altounian Z, Batalla E, Ström-Olsen J O and Walter J L 1987 *J. Appl. Phys.* **61** 149
[10] Nicolaus M M, Sinning H-R and Haessner F 1991 *Mater. Sci. Eng.* at press
[11] Havinga E E, Damsma H and Hokkeling P 1972 *J. Less-Common Met.* **27** 169
[12] Gleiter H 1989 *Progress in Materials Science* **33** 223
[13] Sinning H-R, Nicolaus M M and Haessner F 1989 *Scr. Metall.* **23** 471
[14] Nowick A S and Berry B S 1972 *Anelastic Relaxation in Crystalline Solids* (New York: Academic Press)
[15] Suzuki K, Hayashi N, Tomizuka Y, Fukanaga T, Kai K and Watanabe N 1984 *J. Non-Cryst. Solids* **61–62** 637
[16] Rodmacq B, Mangin Ph and Chamberod A 1985 *J. Phys. F: Met. Phys.* **15** 2259
[17] Kirchheim R 1988 *Habilitationsschrift* University of Stuttgart
[18] Yurko G A, Barton J W and Gordon Parr J 1959 *Acta Crystallogr.* **12** 909
[19] Mütschele T and Kirchheim R 1987 *Scr. Metall.* **21** 135
[20] Zhu X, Birringer R, Herr U and Gleiter H 1987 *Phys. Rev.* B **35** 9085
[21] Sinning H-R, Nicolaus M M and Haessner F 1990 *Proc. RQ* 7; 1991 *Mater. Sci. Eng.* at press